Transferring Compressive-Sensing-Based Device-Free Localization Across Target Diversity

Ju Wang, Xiaojiang Chen, *Member, IEEE*, Dingyi Fang, Chase Qishi Wu, Zhe Yang, and Tianzhang Xing

Abstract—**Device-free localization (DFL) plays an important role in many applications, such as wildlife population and migration tracking. Most of current DFL systems leverage the distorted received signal strength (RSS) changes to localize the target(s). However, they assume a fixed distribution of the RSS change measurements, although they are distorted by different types of targets. It inevitably causes the localization to fail if the targets for modeling and testing belong to different categories. This paper presents TLCS—a transferring compressive sensing based DFL approach—which employs a rigorously designed transferring function to transfer the distorted RSS changes across different categories of targets into a latent feature space, where the distributions of the distorted RSS change measurements from different categories of targets are unified. A benefit of this approach is that the same transferred sensing matrix can be shared by different categories of targets, leading to a substantial reduction in the human efforts. The results of experiments illustrate the efficacy of the TLCS.**

Index Terms—**Compressive sensing (CS), device-free localization (DFL), target diversity, transferring.**

I. INTRODUCTION

THE past few years have witnessed an increasing interests in localizing target(s) that *do not* carry any device, termed as "device-free localization (DFL)" [1]–[6], in contrast to device-enabled localization technologies exemplified by vehicle position system [7] and indoor localization [8]. The DFL has found pervasive use in a variety of applications ranging from intrusion detection [1], privacy-enhanced monitoring [3], [6] to wild animal monitoring [4]. Particularly, DFL for multiple

diverse targets attracts a great deal of attention from zoologists in need of keeping track of wildlife population and migration trajectory, and several techniques have been proposed. The real-time, accurate, and scalable system (RASS) [1] is among the most widely used methods, since it has an advantage of sparse triangular deployment, which can be easily scaled and is cost effective. However, the RASS system fails to localize multiple targets when the targets fall within the same triangle [1]. To cope with the multitarget DFL problem, the radio tomographic imaging (RTI) system [3] is proposed, and it achieves an improved localization performance even through the wall. However, it is at the expense of data volume increase and high energy consumption as it requires any pair of transceivers to sample the received signal strength (RSS) measurements. To address the high energy consumption issue in multitarget DFL, many compressive sensing (CS)-based DFL algorithms, such as those in [4] and [5], have been proposed to localize multiple targets accurately by explicating the sparse property (the multiple targets are sparse in contrast to the number of grids, which are utilized to represent the locations) and the advantage of CS in sparse recovery even in using a small number of RSS measurements.

The key assumption behind these CS-based DFL algorithms is that the RSS change measurements distorted by different categories of targets follow the same distribution, which, unfortunately, is not always true in practical settings. In fact, different categories or types of targets (such as tigers and monkeys in a wild animal monitoring application) are always of disparate shapes and hence yield different distributions of their RSS change measurements. Toward this end, this study conducts preliminary study of the distorted RSS change distributions across diverse targets, as shown in Fig. 1(a).[1] For each category of targets, we collect a set of distorted RSS change measurements when one target of each category is located at the same position and on the same link. Let us consider four targets with different types, i.e., A ($H = 0.6$ m, $W = 0.15$ m), B ($H = 0.3$ m, $W = 0.6$ m), C ($H = 0.3$ m, $W = 0.3$ m), and D ($H = 0$ m, $W = 0.15$ m), where H and W are the effective height and width of each target, respectively. The effective height is equal to the height of the target minus the height of the transceivers. We vary a target's effective height and width by aligning a group of human subjects either half-crouching or standing straight up in a row. The MICAZ [9] nodes are used

---

[1]The purpose of this preliminary study is not to localize the target; thus, the experimental setup is different from Fig. 2, which shows the deployment view for the localization.
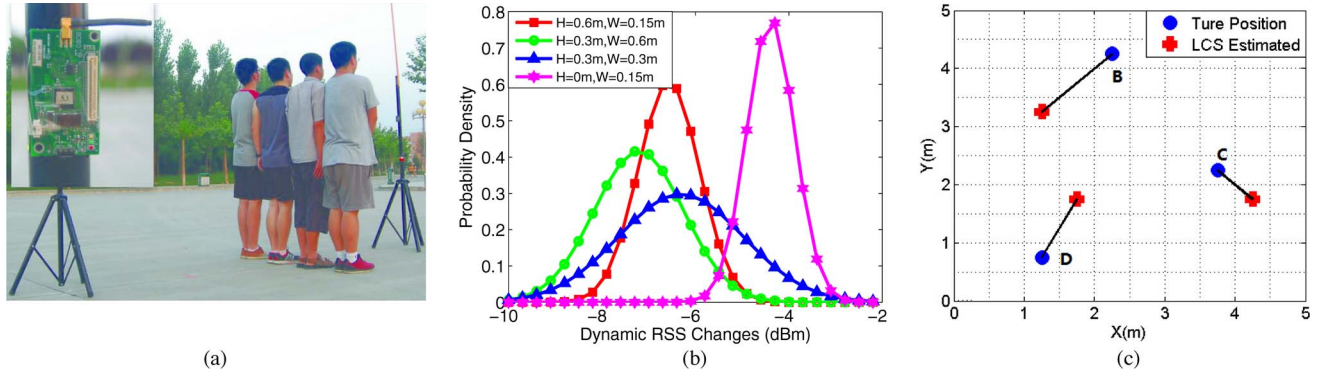
Fig. 1.   Preliminary study of the distorted RSS change distributions and the localization errors caused by the target diversity. (a) Experiment scene. (b) Gaussian estimation. (c) Localization of three target categories.

to set up a wireless link with the length of 4 m. All the MICAZ nodes are placed 0.95 m above the ground. Then, we collect a set of distorted RSS change measurements when one target of each category is located at the middle point of the link. Fig. 1(b) shows that the distributions of the RSS changes distorted by different targets differ significantly from each other even when residing at the same location. This observation implies that the traditional localization models (e.g., trained database [1], [2], [6], shadowing loss [3], or sensing matrix [4], [5]) are bound to fail, if we use one category of targets for building the localization model and another category of targets for testing. For example, Fig. 1(c)[2] shows the localization results of the localization with CS (LCS) algorithm [4] for targets B, C, and D solely based on target A's sensing matrix. Note that, in many cases, it is prohibitively expensive to collect sufficient measurements to build a reasonably accurate localization model for every category of targets. This challenge necessitates a re-examination of the traditional localization methods for reducing the human efforts.

In view of the above limitation, this study considers a more practical method where a small amount of data is collected for a new category of targets and is then integrated with a large amount of data previously collected for other categories of targets. Specifically, two key observations are as follows: 1) The differences in the distorted RSS changes across different target categories are reflected by the differences in their distributions, as shown in Fig. 1(b), and 2) the localization models formulated for different target categories are related as they all reconstruct a sparse location vector using the sensing matrix and a few measurements.

The first observation motivates us to seek for a transferring function that *transfers the measurements of RSS changes* across different categories of targets into a latent feature space, in which the geometric structure of the changes for each target category is preserved, while the distributions of the RSS change measurements from any two target categories are as close as possible. The second observation motivates us to *transfer the original sensing matrix* into the latent space where different categories of targets can share a unified transferred sensing matrix to avoid rebuilding a new sensing matrix.

Without transferring, it is rather difficult to establish an omnipotent trained database, a shadowing loss, or a sensing matrix to localize disparate categories of targets. Thus, according to the preceding observations, this paper presents a transferring CS-based DFL method, referred to as TLCS, to solve the multitarget DFL problem across different target categories *without rebuilding the localization model*, thus saving the human efforts.

The contributions of this work are summarized as follows.

1) This paper initiates a research direction toward the DFL problem across different categories of targets, which is a generalization of the traditional DFL problem for a single category of targets.

2) This paper presents a transferring CS-based DFL method across different categories of targets together with a rigorous proof of its feasibility.

3) This paper justifies that a low-cost linear transformation of RSS changes is sufficient for compensating the differences across different target categories.

4) This paper performs extensive real-life experiments to evaluate the performance of TLCS with various parameter settings. The results illustrate the effectiveness and robustness of the TLCS method and transferring scheme.

This paper would also like to point out that the key idea of TLCS has a wider implication beyond localization across different target categories for solving the similar problems, such as across different space and time domains.

Meanwhile, localizing intensive multiple targets who distort the same link is still an open problem; thus, following most of the current DFL approaches [1]–[6], TLCS will consider intensive multiple targets as a "big" one when they distort the same link. Fortunately, this misidentification event is rare in practice since the effective location area is limited [4].

1) Assumptions: In general, identifying the distorted RSS changes for different targets is a great challenge [1]–[6]. Since the proposed transferring scheme requires a prior knowledge of target categories, this study assumes that one can identify the category of targets.

II. RELATED WORK

The basic idea of RSS-based DFL is to explicate the RSS changes distorted by the target and modeled DFL as a fingerprint-matching (location matched with the RSS changes)

---

[2]The deployment setup follows the work in [13], which uses multiple links to localize the target(s).

problem [1]–[6]. Compared with the similar techniques, such as video-based DFL [10] and ultrasonic-based DFL [11], one main advantage of using RSS for DFL is that the RSS readings are readily available in existing wireless infrastructures and without requiring additional devices (such as camera and ultrasonic sensor). Several research efforts have been devoted to the problem of DFL for multiple targets. Zhang *et al.* [1] proposed the RASS system to perform DFL. They divided the tracking field into grids and used the support vector regression model to localize the object in each area. Wilson and Patwari [3] proposed the RTI system, which exploits the redundancy introduced by sensor arrays surrounding the monitored area to visualize the target induced RSS fluctuations. Since the RSS signal is sensitive and a slight variation of the environment will lead to a large localization error, Wang *et al.* [2] proposed a robust DFL scheme based on the differential RSS, which overcomes the negative effect incurred by the environment. In order to reduce the number of measurements required by DFL systems while maintaining the high localization accuracy, the work in [4] and [5] formulated DFL as a sparse signal reconstruction problem by taking advantage of CS in sparse recovery to handle the sparsity property of the localization problem. The preceding efforts have achieved a good performance in solving the traditional DFL problem.

However, a major drawback of the traditional localization methods is that they assume a fixed distribution of RSS changes distorted by different categories of targets, so that the trained database [1], [2], [6], the shadowing loss [3], or the sensing matrix [4], [5] modeled on one target category can be used for others. This drawback poses a fundamental limitation on the performance of traditional DFL methods, since without transferring, it is rather difficult to establish an omnipotent trained database, shadowing loss, or sensing matrix to localize disparate categories of targets. This study attempts to transfer the original localization framework to a latent space where diverse targets can be treated in a unified framework.

III. TRANSFERRING CS-BASED DFL

This section presents the basic idea of the transferring CS-based DFL algorithm under the LCS [4] framework. This study chooses LCS as its deployment is sparser than other CS-based DFL methods [5] and requires fewer measurements.

A. Outline of LCS

Consider K targets randomly located in an isotropic free space of size $a \times b$, which is equally divided into N grids of edge length ω. Divide $2M$ nodes into two groups, i.e., a TX-node group $\{TX_1, \ldots, TX_i, \ldots, TX_M\}$ and an RX-node group $\{RX_1, \ldots, RX_{i'}, \ldots, RX_M\}$, which are then deployed on both sides of the monitoring area, respectively. Each node is placed at the midpoint of a grid edge, as illustrated in Fig. 2. This study considers a pair of TX_i and $RX_{i'}$ as a link only if $i = i'$. Therefore, there is a total of M links. Since the monitoring area has been divided into N grids, let the locations of K targets over N grids be denoted by vector

$$\Theta = [\theta_1, \ldots, \theta_j, \ldots, \theta_N]^T \qquad (1)$$
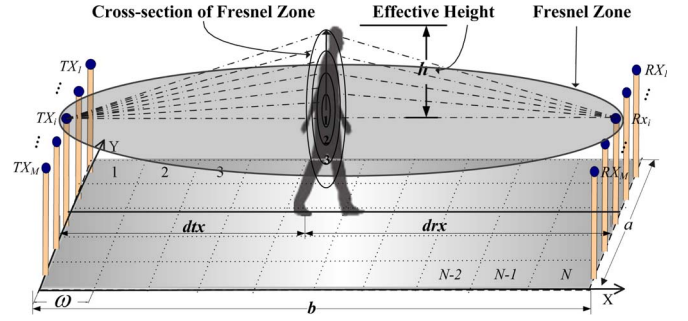

Fig. 2. Deployment view for the localization.

where $\theta_j \in \{0, 1\}$. If there is one target located at grid j, $\theta_j = 1$; otherwise, $\theta_j = 0$. The vector Θ has a K-sparse nature [4], i.e., $K \ll N$, and only K elements of Θ are nonzero. According to the CS theory, rather than measuring the N-dimensional K-sparse signal Θ directly, RSS change measurements $Y_{M \times 1}$ in an M-dimensional space are collected to recover Θ, i.e.,

$$Y_{M \times 1} = A_{M \times N} \cdot \Theta_{N \times 1} + n \qquad (2)$$

where n is the measurement noise. $A_{M \times N}$ is the sensing matrix, under which the measured signal $Y_{M \times 1}$ has sparse coefficient vector Θ. In LCS [4], the sensing matrix is defined as $A_{M \times N} = (r_{i,j})$, where $r_{i,j} \in \mathbb{R}^{M \times N}$ is the RSS change distorted by a target located at grid j and measured by link i in the pre-deployment phase; the measurements are defined as $Y_{M \times 1} = (o_{i,1})$, where $o_{i,1} \in \mathbb{R}^{M \times 1}$ is the RSS change measured by link i in the localization phase. For the $N \times 1$ sparse location vector Θ, it has been proved that if A holds, the restricted isometry property (RIP) and the number of measurements obey $M = O(K \log(N/K))$ [12]; then, the vector Θ can be exactly obtained from the ℓ_1-minimization with relaxed constraints, i.e.,

$$\min \|\Theta\|_{\ell_1} \text{ subject to } \|A\Theta - Y\|_{\ell_2} < \epsilon \qquad (3)$$

where ϵ bounds the amount of noise in the measurements, and its value depends on the empirical knowledge. Following Wang *et al.* [4], [5], this study sets the value of ϵ as 2 dBm. It has been proved [13] that the reconstruction error of Θ based on the value computed from (3) is bounded by $c_0 \epsilon_0 + c_1 \epsilon$, where c_0 and c_1 are small constants, and ϵ_0 is the reconstruction error when Y is noiseless.

B. Framework of TLCS

The design of the sensing matrix is important for accurate recovery of the location vector Θ [4], [5], [12]. For different categories of targets, the established sensing matrix is completely different due to the different RSS change $r_{i,j}$, as illustrated in Fig. 1(b). This observation implies that the traditional CS-based localization model is bound to fail, if the categories of targets used for sensing matrix construction and target localization are different. In practice, the RSS changes $r_{i,j}$ are affected not only by the target category but also by the environmental dynamics. In order to better understand the RSS change distorted by different categories of targets rather than the noise, one must take into

account the variability of the environment. Thus, in this work, we collect Q continuous $r_{i,j,q}$, $1 \leq q \leq Q$, samples, which are denoted by $R_{i,j} = \{r_{i,j,q}\}$, and then have the following 3-D sensing matrix:

$$A_{M \times N \times Q} = \begin{bmatrix} R_{1,1} & \cdots & R_{1,N} \\ \vdots & R_{i,j} & \vdots \\ R_{M,1} & \cdots & R_{M,N} \end{bmatrix} \quad (4)$$

and collect Q continuous $o_{i,1,q}$, $1 \leq q \leq Q$, samples, which are denoted by $O_i = \{o_{i,1,q}\}$, and then have the 2-D measurement

$$Y_{M \times 1 \times Q} = [O_1, \ldots, O_i, \ldots, O_M]. \quad (5)$$

Consider that there are T different categories of targets (each category has multiple targets) sparsely located in the monitoring area, and one has the sensing matrix $A_{M \times N \times Q}$ for the lth category of targets. The goal is to accurately localize all the T categories of targets under the transferred sensing matrix for the lth category of targets. One intuitive solution would be to find a transferring function that makes the distributions of $R_{i,j}$ across different categories of targets as close as possible. The detailed discussion on how to find such functions is shown in Section IV. This section focuses on the TLCS framework under the condition of a known transferring function, consisting of two steps as follows.

In the predeployment phase, we are transferring the sensing matrix. Within the effective localization area [4] of link $i(1 \leq i \leq M)$, we randomly choose a grid $j(1 \leq j \leq N)$. From each of the T categories, we choose one target, and thus, we have T different targets. Let each of the T targets stand at the grid j, respectively, and link i measures a set of RSS changes $\{R_{i,j}^1, \ldots, R_{i,j}^T\}$. Based on this set of RSS changes, one can find a set of corresponding transferring functions $\{\phi_1 \ldots, \phi_T\}$. Then, the transferred sensing matrix of the lth category is given by

$$A_{M \times N \times Q} = (\phi_l(R_{i,j})), \qquad 1 \leq l \leq T. \quad (6)$$

In the localization phase, we are transferring the measurements. Suppose that one can identify the kth $(1 \leq k \leq T)$ category of targets located in the localization area, and the transferred measurements are given by

$$Y_{M \times 1 \times Q} = (\phi_k(O_i)), \qquad 1 \leq k \leq T. \quad (7)$$

After the preceding two transferring phases, the distributions of RSS change measurements across different categories of targets have been made as close as possible. In order to acquire the real RSS change in a noisy environment, this study adopts a traditional method, i.e., the real RSS change is the most frequent measured value, i.e.,

$$r_{i,j} = \arg \max_{1 \leq q \leq Q} p\left(\phi(r_{i,j,q})\right) \quad (8)$$

where $p(\cdot)$ is the probability acquired by the histogram or the Gaussian estimation. Another benefit of this step is that it reduces the 3-D sensing matrix $A_{M \times N \times Q}$ and the 2-D measurements $Y_{M \times 1 \times Q}$ into a lower dimensional space, in which one can easily apply the CS theory to reconstruct the location vector

Θ accurately, i.e., localize all the targets of the kth category accurately, while only using the lth category target's sensing matrix.

C. Key Issues

There are two key issues in the design of TLCS as follows.
- *Key issue 1*: How to find the transferring functions that transfer the distributions of RSS changes across different categories of targets as close as possible.
- *Key issue 2*: Since the transferring functions are obtained by randomly choosing a location in the monitoring area, would such transferring functions work out for all the locations in the area.

IV. TRANSFERRING

A. Transferring Problem Formulation

Suppose that there are T categories of targets with disparate shapes denoted by set $H = \{h_1, h_2, \ldots, h_T\}$. Let $R^{h_l} = \{r_1^{h_l}, r_2^{h_l}, \ldots, r_{n_l}^{h_l}\}$, $1 \leq h_l \leq h_T$, and $R^{h_k} = \{r_1^{h_k}, r_2^{h_k}, \ldots, r_{n_k}^{h_k}\}$, $1 \leq h_k \leq h_T$, be two sets of RSS changes that are distorted by a target of the lth category (with the shape of h_l and n_l measurements) and a target of the kth category (with the shape of h_k and n_k measurements) residing at the same location on the same link, respectively. Let $n = \sum_{l=1}^{T} n_l$. Here, the distributions of R^{h_l} and R^{h_k} are different due to the different RSS changes distorted by different categories (shapes) of targets. The goal is to find transferring functions ϕ_l and ϕ_k, with which one can transfer R^{h_l} and R^{h_k} into a latent feature space, where the geometric structure of the RSS changes in each category of targets is preserved, while the RSS distributions of any two categories of targets are made as close as possible.

Obviously, one fundamental question is how to measure the difference between the distributions of R^{h_l} and R^{h_k}. One option would be to use the Kullback–Leibler divergence, as the work in [14] did. However, the RSS changes are usually high dimensional, and it is hard to precisely model the distributions over the two different sets of RSS changes. Hence, this study proposes to use the maximum mean discrepancy (MMD) [15], which can directly measure the distribution distance without density estimation, to quantify the difference in distributions based on the reproducing kernel Hilbert space distance.

Definition 1: Let $\mathcal{F}$ be a class of functions $f : \mathbb{X} \to \mathbb{R}$. Let $\mathcal{P}$ and $\mathcal{Q}$ be probability distributions defined on a domain $\mathbb{X}$, and let $X = (x_1, \ldots, x_m)$ and $Z = (z_1 \ldots, z_n)$ be independent identically distributed samples drawn from distributions $\mathcal{P}$ and $\mathcal{Q}$, respectively. Then, the MMD (empirical estimation) is

$$\text{MMD}[\mathcal{F}, X, Z] = \sup_{f \in \mathcal{F}} \left(\frac{1}{m} \sum_{i=1}^{m} f(x_i) - \frac{1}{n} \sum_{i=1}^{n} f(z_i) \right) \quad (9)$$

where sup is the supremum of a given set.

It follows that the distance of the RSS change distributions between the lth and kth categories of targets is calculated as

$$\text{dist}(R^{h_l}, R^{h_k}) = \left\| \frac{1}{n_l} \sum_{i=1}^{n_l} \phi_l\left(r_i^{h_l}\right) - \frac{1}{n_k} \sum_{i=1}^{n_k} \phi_k\left(r_i^{h_k}\right) \right\|_{\mathcal{H}}^2 \quad (10)$$

which can be simplified as

$$
\text{dist}(R^{h_l}, R^{h_k}) = \text{tr}\left(\Phi^{h_l,h_k}\text{S}^{h_l,h_k}(\Phi^{h_l,h_k})^T\right)
$$
$$
= \text{tr}(\text{S}^{h_l,h_k}\Omega^{h_l,h_k}) \qquad (11)
$$

where $\Phi^{h_l,h_k} = [\phi_l(r_1^{h_l}), \ldots, \phi_l(r_{n_l}^{h_l}), \phi_k(r_1^{h_k}), \ldots, \phi_k(r_{n_k}^{h_k})]$, $\Omega^{h_l,h_k} = (\Phi^{h_l,h_k})^T \Phi^{h_l,h_k}$, and $\text{S}^{h_l,h_k} \in \mathbb{R}^{(n_l+n_k)\times(n_l+n_k)}$ is defined as

$$
\text{S}_{ij}^{h_l,h_k} = \begin{cases} -1/n_l^2, & \text{if } r_i, r_j \in R^{h_l} \\ -1/n_k^2, & \text{if } r_i, r_j \in R^{h_k} \\ -1/(n_l n_k), & \text{otherwise.} \end{cases} \qquad (12)
$$

For all RSS changes of T categories of targets, we summate the distances between any two categories as follows:

$$
\sum_{h_l,h_k} \text{dist}(R^{h_l}, R^{h_k}) = \sum_{h_l,h_k} \text{tr}\left(\Phi^{h_l,h_k}\text{S}^{h_l,h_k}(\Phi^{h_l,h_k})^T\right)
$$
$$
= \text{tr}(\Phi\text{S}\Phi^T) = \text{tr}(\text{S}\Omega) \qquad (13)
$$

where $\Phi = [\phi_1(r_1^{h_1}), \ldots, \phi_1(r_{n_l}^{h_1}), \ldots, \phi_T(r_1^{h_T}), \ldots, \phi_T(r_{n_k}^{h_T})]$, $\Omega = \Phi^T\Phi$, and $\text{S} \in \mathbb{R}^{n\times n}$ is defined as

$$
\text{S}_{ij} = \begin{cases} (T-1)/n_k^2, & \text{if } r_i, r_j \in R^{h_k} \\ -1/n_l n_k, & \text{if } r_i \in R^{h_l} \text{ and } r_j \in R^{h_k}. \end{cases} \qquad (14)
$$

In addition, we have

$$
\Omega = \begin{bmatrix} \left(\phi_1\left(r_1^{h_1}\right)\right)^2 & \cdots & \phi_1\left(r_1^{h_1}\right)\phi_T\left(r_{n_T}^{h_T}\right) \\ \vdots & \vdots & \vdots \\ \phi_T\left(r_{n_T}^{h_T}\right)\phi_1\left(r_1^{h_1}\right) & \cdots & \left(\phi_T\left(r_{n_T}^{h_T}\right)\right)^2 \end{bmatrix}. \qquad (15)
$$

Note that the smaller the value of (13) is, the closer the distributions of the RSS changes between any two target categories are. Thus, the goal can be formulated as the following optimization problem:

$$
\min_{\Omega} \text{tr}(\text{S}\Omega), \quad \text{s.t. } \text{tr}(\Omega) = C \qquad (16)
$$

where C is any positive constant, and $\text{tr}(\Omega) = C$ is introduced to avoid a trivial solution. Note that it does not require the matrix Ω to be universal. The universal matrix Ω guarantees that MMD $[\mathcal{F}, \mathcal{X}, \mathcal{Z}] = 0$, if and only if $X = Z$. However, the goal is to find a function such that X and Z are close, but not necessarily the same. Obviously, S and Ω are $n \times n$ symmetric matrices. S can be expressed as $\text{S} = \text{P}\Lambda\text{P}^T = \sum_{t=1}^n \lambda_t v_t v_t^T$, where $\Lambda = \text{diag}(\lambda_1, \ldots, \lambda_n), 0 \le \lambda_1 \le \cdots \le \lambda_n$, are the eigenvalues, and $|v_t| = 1$ are the eigenvectors. Following Zhu *et al.* [16], we aim to obtain matrix Ω in the form of

$$
\Omega = \sum_{t=1}^n \sigma_t v_t v_t^T, \qquad \sigma_t > \sigma_{t+1}; \quad t = 1, 2, \ldots \qquad (17)
$$

where v_t is the eigenvector of S, corresponding to the tth smallest eigenvalue λ_t. Thus, (16) is transformed into

$$
\min_{\Omega} \text{tr}(\text{S}\Omega) = \min_{\Gamma} \text{tr}(\text{P}\Lambda\text{P}^T\text{P}\Gamma\text{P}^T)
$$
$$
= \min_{\Gamma} \text{tr}(\Lambda\Gamma) = \min_{\sigma_t} \sum_{t=1}^n \lambda_t \sigma_t
$$

$$
\text{s.t. } 0 \le \sigma_t \le 1, \sum_{t=1}^n \sigma_t = C \qquad (18)
$$

where $\Gamma = \text{diag}(\sigma_1, \ldots, \sigma_n)$ is the linear programming solution of (18), which can be obtained by many existing effective methods such as MATLAB toolbox (R2011a).

B. Finding the Transferring Function

Now, the following problem still remains: how to find an appropriate transferring function $\phi_l(\cdot)$ in (13) when we get matrix Ω by (17). This is a challenging problem because of the following: 1) it is difficult to model the correlation between the shape of a target and the distorted RSS changes, which is still an open problem, and 2) it is difficult to find a unique mapping function from a high-dimensional matrix Ω to a low-dimensional polynomial product due to the multiplicity of the inner product. This study attempts to construct an approximate transferring function based on extensive experiments. Since the RSS changes are discrete points, there must exist a differential. According to Taylor's formula, it is well known that $\phi_l(r_i^{h_l})$ can be approximated as

$$
\phi_l\left(r_i^{h_l}\right) \approx a_0^{h_l} + a_1^{h_l} r_i^{h_l} + \cdots + a_m^{h_l}\left(r_i^{h_l}\right)^m \qquad (19)
$$

where $a_0^{h_l} = \phi_l(0)$, and $a_m^{h_l} = \phi_l^{(m)}(0)/m!, m = 1, 2, \ldots$.

Let us examine (15) more closely. Each element of (15) is a product of two polynomials, and the polynomial is formulated as (19). Obviously, Ω is an $n \times n$ symmetric matrix with $n(n+1)/2$ different elements, making it possible to construct $n(n+1)/2$ equations. There is a total of $(m+1)T$ unknown coefficients in (15) since there are $m+1$ unknowns for the lth category of targets in (19). Usually, the number T of targets is smaller than the total number n of RSS changes. This indicates that, by choosing an appropriate order m of (19) (such that $(m+1)T \le n(n+1)/2$), eventually there would be enough constraints to make every transferring function $\phi_l(\cdot), 1 \le l \le T$, uniquely solvable. In fact, some of the elements are close but not exactly equal since none of any pair distributions would be identical. Obviously, these are a set of simultaneous multivariate quadratic equations since the order of all the unknown coefficients in (19) is one. To the best of our knowledge, there exists neither an analytical solution nor any prior work that analyzes them. However, in most practical scenarios, it is possible to determine whether or not the equations are uniquely solvable by checking if the Jacobian of the equations has a full rank (equal to the number of variables) when formulated in the form of $Jy = z$, where J is the Jacobian, y is a vector containing all the unknown parameters, and z is a constant vector. As long as the equations are uniquely solvable, this problem can be formulated as a quadratic programming problem [17] so that all the $m+1$ coefficients of the transferring function $\phi_l(\cdot)$ can be acquired. The quadratic programming problem can be solved by many existing algorithms, such as the work in [17], which find the best least squares fit with a relatively low complexity.

It is difficult to determine an appropriate order m of function $\phi_l(\cdot)$ through theoretical analysis due to the challenges described earlier. Nevertheless, this paper shows that the order
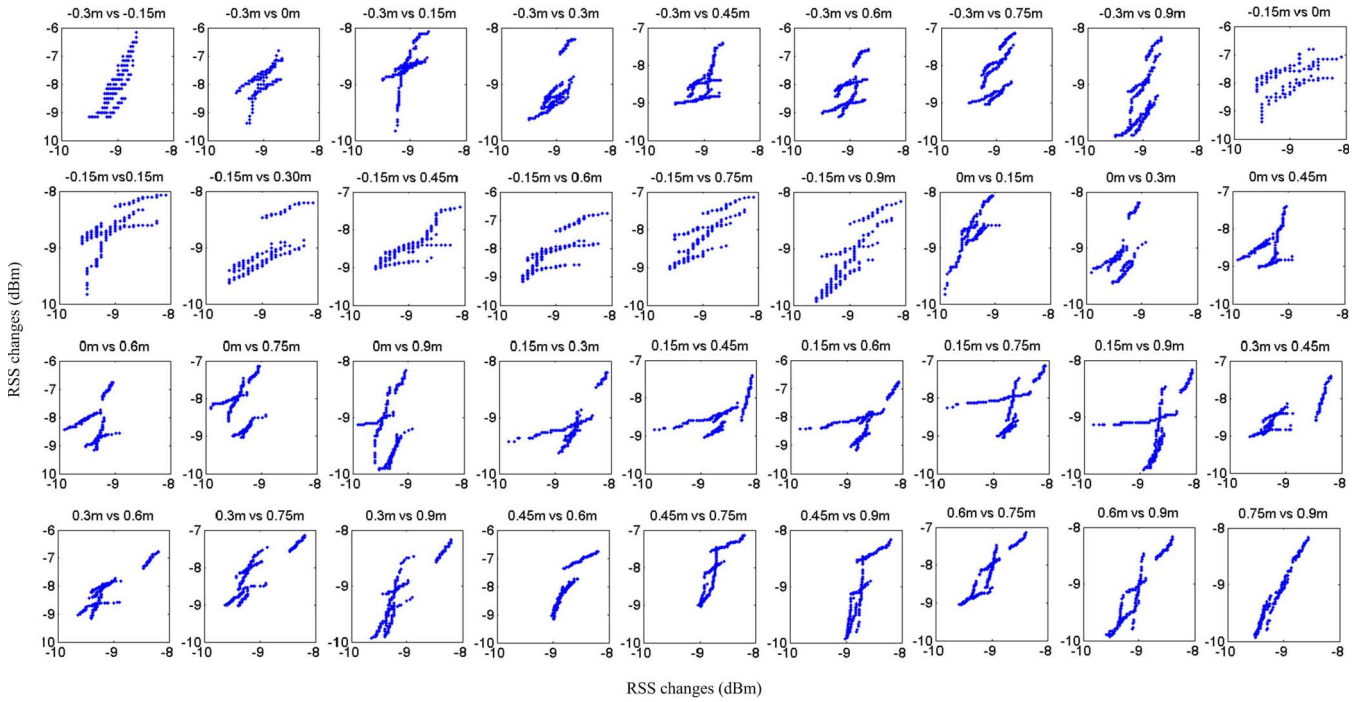
Fig. 3. Each point in each scatterplot represents a pair of RSS change values from two categories of targets.

$m = 1$ achieves good performance in most cases based on extensive empirical studies. Based on a thorough investigation into the impact of different target shapes on the distorted RSS change measurements, we are able to determine the most suitable order m of the transferring function. It is generally infeasible to exhaust all possible cases with limited experiments. However, by carefully choosing three key parameters, we are able to ensure the comprehensiveness of our experimental studies as described in the following.

1) Link Length: The basic idea of the DFL is to use the RSS changes to localize the target [1]–[6]. The longer the link length is, the weaker the distorted RSS changes are [4]. Since the weak RSS changes may be absorbed by the noise, most of the existing DFL work [1]–[6] limit the link length within 10 m. Following that, we set the link length to be $b = 4$ m, and other link lengths are tested in Section V.

2) Target Shape: According to the diffraction theory [18], when the target blocks the propagation path, we can model the signal propagation using the knife-edge diffraction model. If a target blocks the first ellipsoidal Fresnel zone, there will be a great amount of signal attenuation [18]. Since the cross section of the blocked ellipsoidal Fresnel zone is a circle, as illustrated in Fig. 2, the height or the width of a target has similar impact on the RSS changes. Moreover, a target's thickness is equivalent to its width when the target turns $90°$ from facing the transceiver. Hence, we only need to test the changes of height in the first Fresnel zone. The benefit of changing the effective height lies in the fact that we can easily change the shape of a target to ensure the comprehensiveness of our experiments. The maximum radius of the first Fresnel zone in this experiment (on a link length of 4 m) is 0.7 m. We arrange nine human subjects with an effective height of 0.9, 0.75, 0.6, 0.3, 0.15, 0, −0.15, and −0.3 m, respectively, to act as nine different categories of

targets (we change the effective height by asking the human subjects to half-crouch).

3) Test Locations: Since not all the locations where the target stands would distort RSS changes, the test locations must fall within the effective location area [4]. In this paper, we choose five test locations along the line of a single link within the effective localization area. The five test points are $dtx = 1$, 1.5, 2, 2.5, and 3 m, respectively; and dtx is the distance from a test point to the TX node, as illustrated in Fig. 2.

Based on this experiment, the following three observations indicate that the order $m = 1$, i.e., a low-cost linear function, is a reasonable choice.

1) Most pairs of RSS changes across different categories of targets show a strong linear correlation. Since there are nine categories of targets with disparate shapes, we have a total of 36 pairs of combinations between any two categories. Fig. 3 plots the RSS changes for each pair of the two categories; as we can see, it shows a strong linear correlation. For example, the scatterplot in row 3, column 2 compares the RSS change values of the two categories of targets with an effective height of 0 and 0.75 m, respectively.

2) The linear function significantly reduces the differences in distributions of RSS changes across different categories of targets. Note that the goal is to minimize the MMD across different categories of targets. Fig. 4 shows the impact of the order m on the MMD. The MMD declines drastically when the order m increases from 0 to 1. However, the MMD is not sensitive to larger values of m. For example, the decrease in MMD is merely 6.25% as m increases from 1 to 2 and remains almost unchanged for $m \geq 3$.
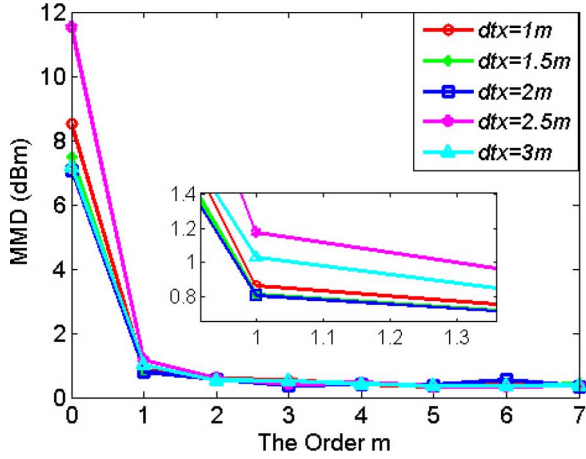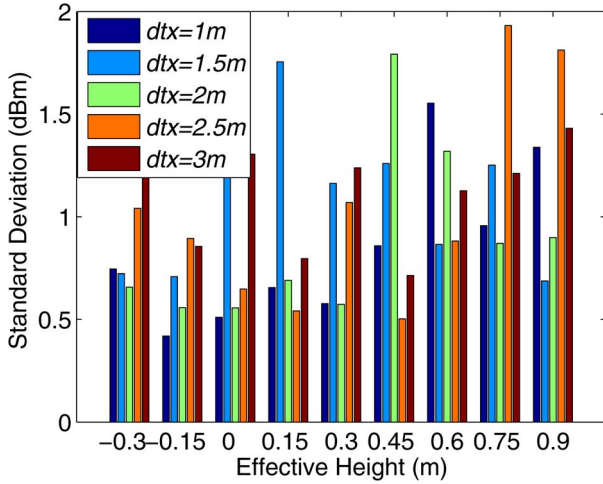
Fig. 4. Impact of the order m.

Fig. 5. Impact of the effective height.

3) The error caused by the linear function is absorbed by the noise. Fig. 5 shows the impact of the effective height on the standard deviation of the RSS changes. We observe that the maximum standard deviation is under 2 dBm, i.e., the noise is bounded under 2 dBm. The MMD decreases to 0.8 dBm when the order $m \geq 2$. This reduction is trivial and is already mixed into the noise.

C. Compensation With the KDE

Based on the transferring function described above, Fig. 6 depicts the transferring performance across four targets described in Fig. 1(b). The mean values of these four distributions are similar, but the variances are quite different. The discrepancy in the variances is mainly caused by the noise of individual samples, such as the absorption differences and variations over time. In order to mitigate such differences in distributions, this study considers kernel density estimation (KDE) for compensation as it takes the noisiness of individual samples into account. The kernel density estimator $\hat{p_R}(\cdot)$ [19] estimates the probability density function $p_R(\cdot)$ as follows:

$$\hat{p}_R(r) = \frac{1}{L_R \cdot W} \sum_{i=1}^{L_R} K\left(\frac{r - r_i}{W}\right) \quad (20)$$
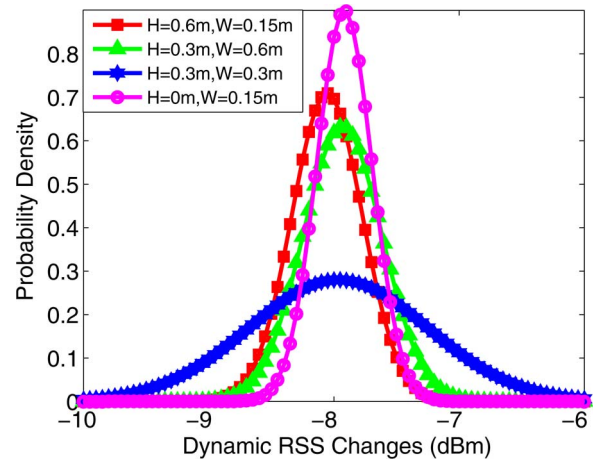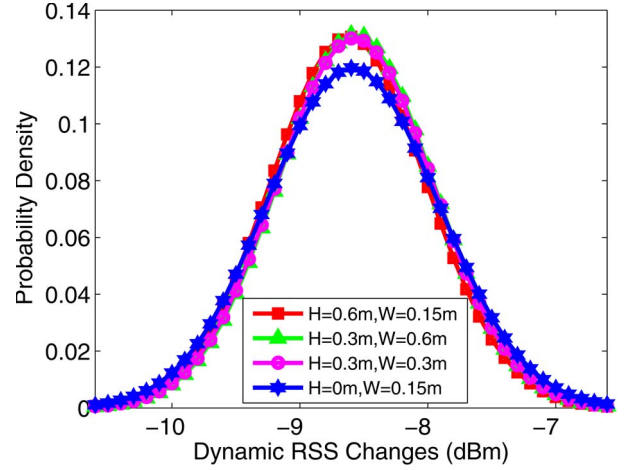

Fig. 6. Gaussian estimation.

Fig. 7. Kernel estimation.

where r_i is an observed sample of random variable R, L_R is the length of variable R, W is the kernel width, and $K(\cdot)$ is the kernel function. This study uses the Gaussian kernel as the kernel function since most of the RSS changes fit the log-normal distribution [2], [4], as shown in Fig. 1(b).

Fig. 7 illustrates the effectiveness of using KDE to compensate different distributions across different categories of targets. A kernel width of 4 dBm is used in this experiment, whereas the best kernel width is tested in Section V.

D. Performance Analysis

This subsection provides a theoretical proof to address the second key issue and show that our transferring scheme works well for all the grids of the monitoring area.

Theorem 1: If the transferring function is linear, most of the greedy CS recovery (GR) algorithms reconstruct Θ correctly, i.e., output $\hat{\Theta} = \Theta$.

Proof: The key idea of the GR algorithms is to minimize the term $\|Y - A\Theta\|_2^2$ with respect to Θ[20]. For TLCS, the GR can be written as

$$\min \|\phi(Y) - \phi(A)\Theta\|_2^2 \quad (21)$$

where $\phi(Y)$ and $\phi(A)$ are the shorthands of (7) and (6), respectively. Since the transferring function $\phi(\cdot)$ is linear, (21)

can be rewritten as

$$\min \|a(Y - A\Theta + b)\|_2^2 = \min \|Y - A(\Theta - A^{-1}b)\|_2^2 \quad (22)$$

where a and b are real numbers. We consider proof by induction. We first prove that the GR generates the correct prediction at the first iteration. Note that, if there are targets on grid i, there must exist $z_i > 0$, $\|z_i - \Theta\|_2^2 = \|\Theta - z_i\|_2^2 \leq \|\Theta\|_2^2 - 1$. Based on [4], sensing matrix A satisfies RIP with $\delta < 1/K$, and we have

$$\|\phi(Y) - \phi(A)\Theta\|_2^2$$
$$= \left\|A\left(z_i - (\Theta - A^{-1}b)\right)\right\|_2^2 \quad (23)$$
$$\leq (1+\delta)\left\|z_i - (\Theta - A^{-1}b)\right\|_2^2 \quad (24)$$
$$\leq (1+\delta)\left(\|\Theta - A^{-1}b\|_2^2 - 1\right). \quad (25)$$

In addition, note that, if there is no target on grid j but the GR chooses $z_j > 0$, $\|z_j - \Theta\|_2^2 = \|\Theta - z_j\|_2^2 \geq \|\Theta\|_2^2 + 1$, we have

$$\|\phi(Y) - \phi(A)\Theta\|_2^2$$
$$= \left\|A\left(z_j - (\Theta - A^{-1}b)\right)\right\|_2^2 \quad (26)$$
$$\geq (1-\delta)\left\|z_j - (\Theta - A^{-1}b)\right\|_2^2 \quad (27)$$
$$\geq (1-\delta)\left(\|\Theta - A^{-1}b\|_2^2 + 1\right). \quad (28)$$

Since $\|\Theta\|_2^2 \geq K$ and $\delta < 1/K$, we have

$$\frac{\left\|A\left(z_i - (\Theta - A^{-1}b)\right)\right\|_2^2}{\left\|A\left(z_j - (\Theta - A^{-1}b)\right)\right\|_2^2} \leq \frac{(1+\delta)\left(\|\Theta - A^{-1}b\|_2^2 - 1\right)}{(1-\delta)\left(\|\Theta - A^{-1}b\|_2^2 + 1\right)} < 1. \quad (29)$$

Thus, there exists i with $\Theta_i \geq 1$ for all j with $\Theta_j = 0$ such that $\|A(z_i - (\Theta - A^{-1}b))\|_2^2 < \|A(z_j - (\Theta - A^{-1}b))\|_2^2$. This indicates that GR generates the correct prediction at the first iteration.

Let us suppose that GR generates the correct prediction at the first u iterations. To prove the correctness of the $(u+1)$th iteration, a key observation is that, given $\delta < 1/K$, we know $\delta < 1/(K-u)$ for all $u \geq 0$. At the $(u+1)$th iteration, we define a $1 \times N$ vector Θ' such that $\Theta_i' = \Theta_i$, if there are targets on grid i and z_i has not yet been identified at the first u iterations, and $\Theta_i' = 0$. We have $\|\Theta' - z_i\|_2^2 \leq \|\Theta'\|_2^2 - 1$, iff $\Theta_i' > 0$. If no target is located at grid j, we have $\|\Theta' - z_j\|_2^2 \geq \|\Theta'\|_2^2 + 1$. Similar to the derivations in (25) and (28), we have

$$\frac{\left\|A(z_i' - (\Theta - A^{-1}b))\right\|_2^2}{\left\|A(z_j' - (\Theta - A^{-1}b))\right\|_2^2} \leq \frac{(1+\delta)\left(\|\Theta' - A^{-1}b\|_2^2 - 1\right)}{(1-\delta)\left(\|\Theta' - A^{-1}b\|_2^2 + 1\right)} < 1. \quad (30)$$

Thus, GR generates the correct prediction at the $(u+1)$th iteration. In summary, GR accurately predicts the locations of all the targets as long as the transferring function is linear. ∎

This study applies the greedy matching pursuit (GMP) [21] to recover the sparse location vector, since GMP recovers signals without requiring the sparsity level, i.e., the number K of targets is generally unknown in practical applications.

Fig. 8.   Experiment scene.

V. DEPLOYMENT AND RESULTS

A. Experimental Setup

We conduct extensive experiments in an open space of size 4 m × 4 m, as depicted in Fig. 8. Based on the work in [4], we set the grid length $\omega = 0.5$ m. We use the MICAZ [9] nodes as the transceivers, which exhibit a relatively good propagation performance when they are 0.95 m above the ground based on our empirical studies, and the similar setup also can be seen in [2]–[5]. In each localization experiment, every link records 30 measurements. We attempt to localize three categories of targets ("category 1"{A, B}, "category 2"{C, D}, and "category 3"{E}) under the condition of only knowing the sensing matrix of category 3. We arrange five human subjects that act as the targets. As we described before that the height or the width of a target has similar impact on the RSS changes, thus, we only consider the differences in height. The targets A, B, C, D, and E have different effective heights of 0.3, 0.3, 0.6, 0.6, and 0.8 m, respectively. Unlike most of the existing work [1]–[6], which assume that the targets are located at the center of a grid, the targets in our experiment are randomly positioned in the grid, which reflects a more realistic scenario.

Comparisons: We implement two state-of-the-art algorithms for comparison, i.e., the RASS [1] and RTI [3] algorithms. In order to show the improvement in localization accuracy made possible by our transferring scheme and better illustrate the effectiveness of the TLCS algorithm, we add our transferring scheme into the RASS and RTI algorithms and refer to them as RTI w/Trans. and RASS w/Trans., respectively.

We evaluate the performance by adjusting the following parameters: 1) M: the number of links; 2) K: the number of targets; 3) m: the order of transferring function ϕ; 4) W: the kernel width; 5) C: the constant in (16); 6) b: the length of link; and 7) As: the size of localization area. Unless mentioned otherwise, the default values in Table I are used.

B. Localization Accuracy and Energy Consumption

Here, we attempt to localize the two categories of targets {A, B} and {C, D}, respectively, using the sensing matrix of category 3. Each category of targets is tested in 15 runs of localization.

TABLE I
DEFAULT VALUES OF EXPERIMENTAL PARAMETERS

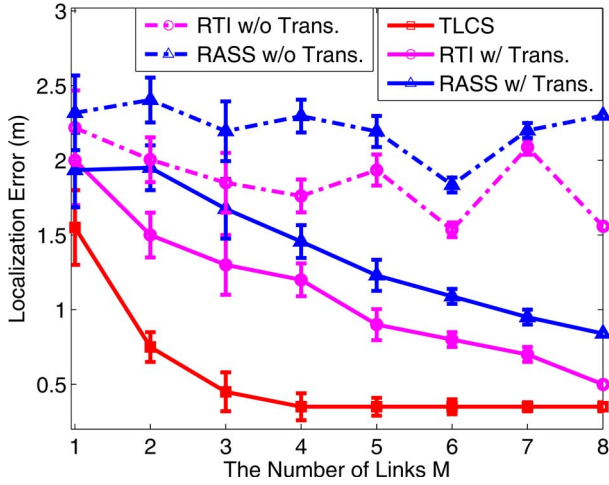| Parameters	Default Values
The number M of links	8
The number T of categories	3
The number K of targets	2,2,1
The order m	1
The kernel width W	4 dBm
The constant C	$65^2 \times 100 \times 5$
The length b of link	4m
The size As of area	4×4m

Fig. 9.   Impact of link count.

Fig. 10.   Impact of target count.

Fig. 11.   Localization performance.

First, we evaluate the feasibility of a sparser deployment. We decrease the number M of links from 8 to 1, by randomly removing the links deployed on two sides of the monitoring area while other parameters use the default values. As shown in Fig. 9, compared with the default deployment scenario, the result indicates that TLCS supports a sparser deployment with a particular number of targets, e.g., the localization error of TLCS still maintains a smaller value when $M = 4 < 8$, as it still satisfies $M = 4 > K(\log(N/K)) = 3.01$ according to the CS theory. RTI w/Trans. and RASS w/Trans. do not perform as well because they require a denser deployment to collect sufficient measurements to localize the target accurately [1], [3]. The reason that TLCS outperforms RTI w/o Trans. and RASS w/o Trans. will be explained in Fig. 11.

This experiment investigates how many targets can be accurately localized by TLCS. We increase the number K of targets from 1 to 8 (all the targets are from category 2), whereas other parameters use the default values, except for the number of links, which is set to be 5. As shown in Fig. 10, the maximum number of targets that can be accurately localized by TLCS depends on the number of links, i.e., under the restriction of $M > K(\log(N/K))$. For example, when $K > 5$, the number of links required is $K(\log(N/K)) \approx 5.6$, which is larger than what we have deployed in this scenario. For the similar reason, TLCS outperforms the RTI w/Trans., RTI w/o Trans., RASS w/Trans., and RASS w/o Trans. algorithms.

Fig. 11 shows the cumulative distribution function (CDF) of localization errors. TLCS performs the best with 50th and 80th percentile errors of 0.5 and 0.7 m, respectively, whereas RTI w/o 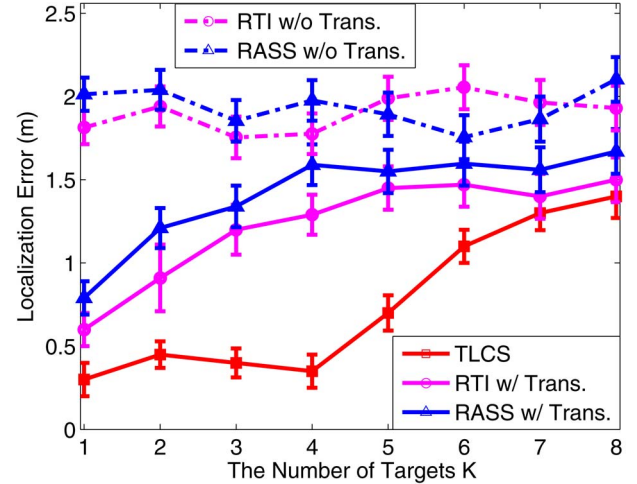Tran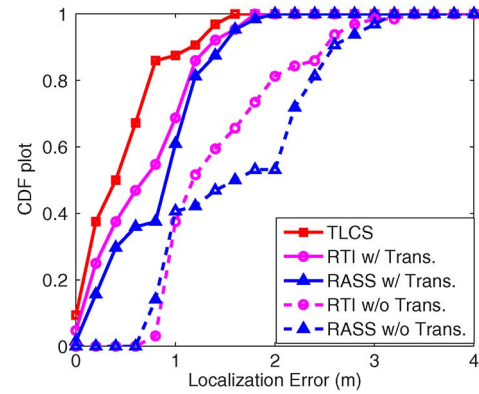s. and RASS w/o Trans. yield a large error with values of 1.8 m (80th percentile) and 2.2 m (80th percentile), respectively. The poor performance of RTI w/o Trans. and RASS w/o Trans. is mainly due to the fact that the trained database of RASS and the shadowing loss of RTI are quite different across all the three categories of targets. Fig. 11 also shows that the performance of the RTI and RASS algorithms is significantly improved by our transferring scheme, for example, the 80th percentile errors of RTI w/Trans. and RASS w/Trans. decrease from 2 and 2.5 m to 0.9 and 1.2 m, respectively.

Here, we compare the energy consumption among TLCS, RASS, and RTI under a given localization accuracy. For a fair comparison, we add the transferring scheme into RASS and RTI, i.e., compare TLCS with RTI w/Trans. and RASS w/Trans. For each method, we increase the number of links until the localization accuracy reaches the given value and then calculate the energy consumption. Based on the first-order radio model [22], the energy consumption for each link is calculated as $E_{\mathrm{radio}} = e_l B b^2 + 2B E_{\mathrm{elc}}$, where B is the size of a packet in bits, b is the link length, $e_l = 100$ pJ/bit/m², and $E_{\mathrm{elc}} = 50$ nJ/bit. In our experiments, $B = 320$ bit, $b = 4$ m, and we repeatedly send 30 packets each time. Thus, the energy consumption of a method with the number M of links is $M \times 0.96$ mJ. Fig. 12 shows the energy consumptions under different average localization errors. To achieve a given accuracy, TLCS consumes the least energy, whereas RTI w/Trans.
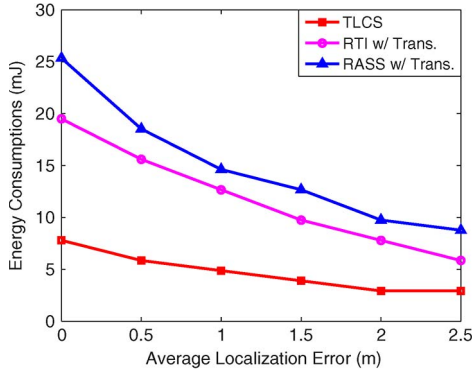
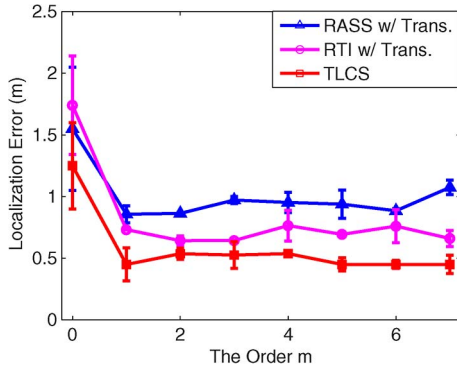Fig. 12.   Comparison of energy consumptions.

Fig. 14.   Impact of kernel width.

Fig. 13.   Impact of function order.

Fig. 15.   Impact of constant C.

and RASS w/Trans. consume more energy. The reason is that TLCS employs CS to localize targets accurately even with just a small number of measurements, whereas RTI and RASS require more measurements for an accurate localization. Fig. 12 also shows that the energy consumption increases as the localization error decreases. The reason is that the more links there is, the less the localization error is [1], [4], as shown in Fig. 9.

C. Impact of the Parameters in a Transferring Function

We discuss the most critical parameters used in our transferring scheme, i.e., the order m, the kernel width W, and the constant C in (16). Each category of targets is tested in 15 runs of localization. Fig. 13 shows the localization errors under different order m. For all these three methods, the localization accuracy does not change significantly when the order m is larger than 1. This indicates that the order $m = 1$ is capable of compensating the differences across different targets. Fig. 14 shows the localization errors under different kernel widths. A kernel width of 3.5 dBm provides the best localization performance in this experiment. Not surprisingly, the effect of kernel estimation is also significant for different categories of targets, as their deviation is large, as shown in Fig. 5. A strategy of doing more "smoothing" than that required for single-target localization is more effective. Fig. 15 shows the localization errors under different constant C. The localization error of all methods does not vary significantly as C only restricts the transferring space size, and it does not change the "matching" between the sensing matrix and the measurements.
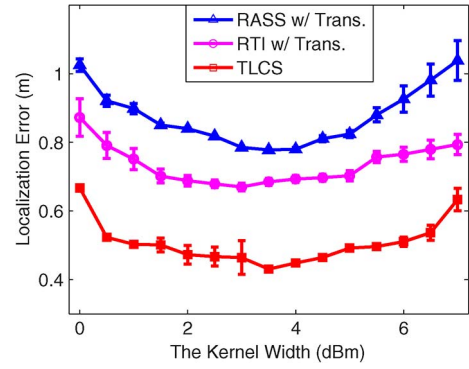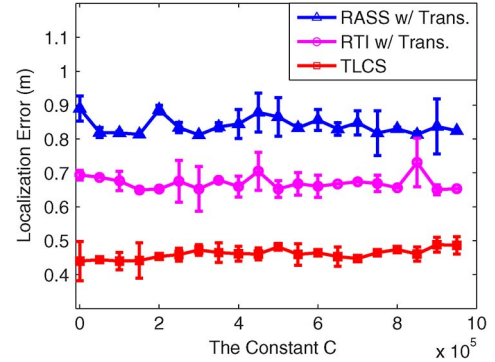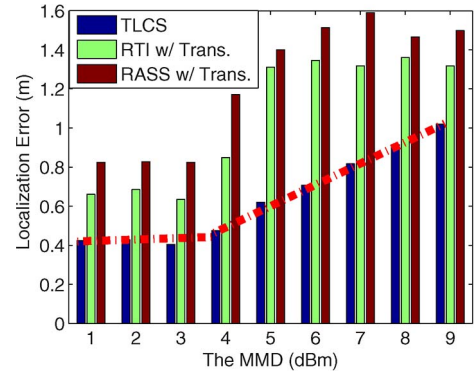

Fig. 16.   Performance of new target.

D. Robustness of TLCS

Here, we evaluate the robustness of the TLCS algorithm through the following two experiments.

This experiment investigates the performance of TLCS when it localizes a new category of targets that are not used for modeling the transferring function. A new target category means a new MMD across the existing categories of targets; thus, we only need to investigate how does the difference of MMD among targets affect the localization performance. To answer these questions, we purposefully add white Gaussian noise to the RSS changes of category 1 (targets A and B) after the transferring. Fig. 16 shows the average localization errors under different values of MMD. We observe that TLCS outperforms the other two schemes, no matter how the MMD is scaled. An interesting observation is that when the MMD is larger than 4 dBm,
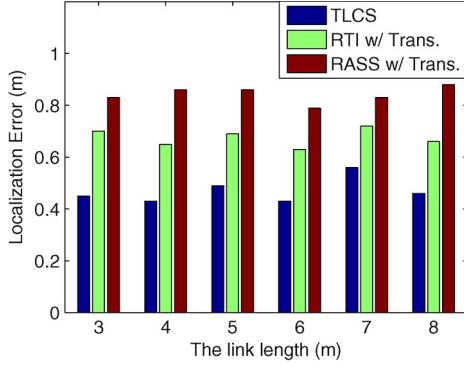
Fig. 17. Performance of other link lengths.

Fig. 18. Time–cost under different categories.

the localization error of TLCS increases linearly, whereas for the other two algorithms, the error remains almost at a large constant value. According to [23], if the measurement error or noise is power limited to ϵ, the reconstructed signal $\hat{\Theta}$ is guaranteed to be within $\delta\epsilon$ of the original signal $\hat{\Theta}$, i.e., $\|\hat{\Theta} - \Theta\|_{\ell_2} \leq \delta\epsilon$, where the constant δ depends only on the measurement parameters, not on the level of noise. Since the MMD quantifies the bound of the measurement noise, the localization error of TLCS increases linearly as the MMD varies linearly.

Since all the experiments we conduct above are under the link length of $b = 4$ m, the localization area is limited to 4 m × 4 m. To investigate the performance of TLCS and our transferring scheme under other link lengths and other area sizes, we conduct additional experiments, with a link length of $b = 3$ m (area size of 3 m × 3 m), 4 m (area size of 4 m × 4 m), 5 m (area size of 5 m × 5 m), 6 m (area size of 6 m × 6 m), 7 m (area size of 7 m × 7 m), and 8 m (area size of 8 m × 8 m), respectively. In each experiment, we use the same implementation and deployment settings as described earlier, except for the link length. Since these experiments require a significant amount of human efforts, we only randomly test 20 grids in each experiment due to the time and resource constraints. Fig. 17 shows the average localization errors under six different link lengths, and we observe that all the three localization methods achieve a stable accuracy performance and that TLCS performs the best. These experimental results indicate that TLCS and our transferring scheme perform well under different link lengths.

E. Reducing the Human Efforts With Transferring

In order to examine how much human effort can be reduced by our transferring scheme, we compare the time–cost of the predeployment in the conditions with and without our transferring scheme, respectively. Traditionally, R_{ij} of the sensing matrix [in the form of (4)] is acquired manually, i.e., one target stands at the grid j and the link i records the corresponding Q continuous RSS change measurements. It takes a lot of human hours to build the sensing matrix this way. Fig. 18 shows the time–cost under different categories of targets in a 10 m × 10 m area. The area is divided into grids with the edge length of 0.5 m, and we collect 30 continuous measurements at each grid, and each transceiver transmits one packet every second. Then, the time–cost for one category of targets to establish the sensing
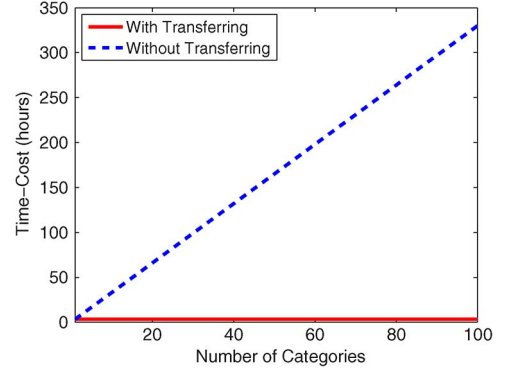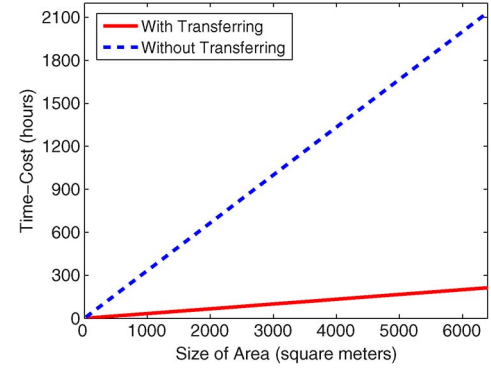

Fig. 19. Time–cost under different sizes of area.

matrix is at least $(30 \times (10/0.5)^2)/3600 \approx 3.3$ man hours. For T categories of targets, the time–cost is at least 3.3 T man hours without our transferring scheme. In contrast, there is almost no extra time–cost (still about 3.3 h) with our transferring scheme. Note that the maximum time–cost (when $T = 100$) to calculate the transferring function and the transferred sensing matrix is only 0.5 h (we test it using MATLAB 7.0 on an Acer laptop with 2.0-GHz central processing unit and 4-GB memory), which can be ignored compared with 340 h when $T = 100$. Moreover, we also compare the time–cost under different sizes of areas in Fig. 19, which shows that the time–cost generally increases as the area scales up, whereas our transferring scheme is still able to reduce a great number of human hours.

F. Scalability of TLCS

As mentioned in Section IV, most of the existing DFL methods [1]–[5] limit the link length within 10 m, which leads to a limited monitoring area. In recent years, many solutions [1], [2], [4], [5] have been developed to deal with this limitation. The basic idea is to divide a large area into a small number of subareas and then apply the localization method, such as TLCS, in each subarea. Since TLCS is under the framework of LCS [4] method, we use the scalable approach introduced in LCS. In order to evaluate the scalability of TLCS, we increase the size of the localization area from 4 m × 4 m to 8 m × 8 m and the number K of targets from 5 to 30. For simplicity, we still set the size of each subarea to be 4 m × 4 m. All the K targets are from category 2, whereas the sensing matrix of category 3 is used for localization. Fig. 20 shows the average

	K=5	K=10	K=15	K=20	K=25	K=30
4mX4m	0.31	0.67	1.20	1.54	1.67	1.73
4mX8m	0.16	0.33	0.45	0.66	1.34	1.50
8mX8m	0.10	0.17	0.22	0.28	0.31	0.43

Fig. 20.   Scalability of TLCS.

localization errors under different sizes of areas and different numbers of targets. It illustrates that the maximum area where TLCS is applicable relies on the maximum number of targets. For example, when $K = 15$, the localization error increases drastically in the 4 m × 4 m area, whereas the error is still small in the 8 m × 8 m area. The reason is that the maximum number of targets that can be precisely localized in each subarea is less than 10, since $K \log(N/K) \approx 8.1 > 8$ when $K = 10$ and $N = (4/0.5)^2$. Therefore, the maximum numbers of targets that can be precisely localized in the 4 m × 4 m and 8 m × 8 m areas are 10 ($< K = 15$) and 20 ($> K = 15$), respectively. Thus, the localization error is large in the 4 m × 4 m area, whereas the error is small in the 8 m × 8 m area.

Since these experimental results show that the maximum area where TLCS is applicable relies on the maximum number of targets, here, we provide some analyses and discussions about the scalability of TLCS. Based on the CS theory [12] and the experimental results shown in Fig. 10, there exists a maximum number $K_{\max}$ of targets that can be precisely localized in each subarea. Considering a large monitoring area, which is divided into ξ subareas, the maximum number of targets randomly located in the area that can be precisely localized is less than $\xi K_{\max}$. If the maximum number of targets in the monitoring area is less than $\xi K_{\max}$, TLCS can scale to any area size with high localization accuracy. Otherwise, the localization error has the following two characteristics: 1) If the area size is fixed, more targets lead to higher localization errors, and 2) if the number K of targets is fixed, larger area sizes lead to lower localization errors, as illustrated in Fig. 20.

VI. DISCUSSION

A. Solutions for the Assumption

Since the proposed TLCS scheme requires a prior knowledge of target categories, this study assumes that one can identify the category for any target located in the monitoring area. According to the diffraction theory [18], the distorted RSS change measurement r can be expressed as $r = f(H, d_{tx}, d_{rx})$, where $f(\cdot)$ is the Fresnel integral function; H is the effective height of target; and d_{tx} and d_{rx} are the distances from the target to the TX and RX nodes, respectively. Based on the measurement r, it is a challenge to identify the target category, i.e., determine the effective height H, since we do not know the location of the target, i.e., the distances d_{tx} and d_{rx}. For

example, a large RSS change measurement may be caused by a small target that is close to the transceiver or a large target that is far away from the transceiver; thus, it is a challenge to determine whether the target is small or large. One approach to this problem is to construct a "DFL profile" for each target category that characterizes the targets in the same category. For example, Xi et al. [24] constructed a channel state information (CSI) profile model for different categories of targets and then determined the sizes of different targets by analyzing the CSI characteristics.

B. Impact of the Environment and the Assumption

In real-world applications, the environment may have some negative effects on the identification of the target category. For example, the noise may lead to an incorrect identification. On the other hand, if this assumption is not satisfied, it may also result in an incorrect identification. If a target is incorrectly identified, as long as the target belongs to one of the known categories, TLCS is still able to localize the target accurately since the transferring function still works well in this case. However, if the incorrectly identified target category is not among the known ones, it would become a test for the robustness of TLCS, which is discussed in Section V-D.
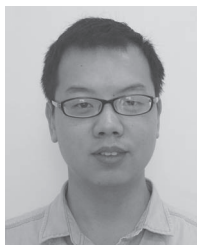
VII. CONCLUSION

This paper has identified the multiple-target DFL problem across different categories of targets based on transferring CS. This paper has investigated the impact of target diversity on the RSS changes distorted by different categories of targets and has shown that most pairs of RSS changes across different shapes of targets show a linear correlation. Thus, we use a linear function to compensate the difference between different targets and prove that our transferring scheme works well for our TLCS method. Additionally, the results of experiments illustrate the effectiveness and robustness of the proposed TLCS method.

REFERENCES

[1] D. Zhang, Y. Liu, X. Guo, and L. M. Ni, "RASS: A real-time, accurate, scalable system for tracking transceiver-free objects," IEEE Trans. Parallel, Distrib. Syst., vol. 24, no. 5, pp. 996–1008, May 2013.

[2] J. Wang et al., "Robust device-free wireless localization based on differential RSS measurements," IEEE Trans. Ind. Electron., vol. 12, no. 60, pp. 5943–5952, Dec. 2013.

[3] J. Wilson and N. Patwari, "See-through walls: Motion tracking using variance-based radio tomography networks," IEEE Trans. Mobile Comput., vol. 10, no. 5, pp. 612–621, May 2011.

[4] J. Wang et al., "LCS: Compressive sensing based device-free localization for multiple targets in sensor networks," in Proc. 32nd IEEE INFOCOM, Turin, Italy, Apr. 2013, pp. 145–149.

[5] J. Wang, Q. Gao, X. Zhang, and H. Wang, "Device-free localisation with wireless networks based on compressive sensing," IET Commun., vol. 6, no. 15, pp. 2395–2403, Oct. 2012.

[6] J. Wang, Q. Gao, P. Cheng, L. Wu, and H. Wang, "Lightweight robust device-free localization in wireless networks," IEEE Trans. Ind. Electron., vol. 61, no. 10, pp. 5681–5689, Oct. 2014.

[7] S. Park and H. Lee, "Self-recognition of vehicle position using UHF passive RFID tags," IEEE Trans. Ind. Electron., vol. 60, no. 1, pp. 226–234, Jan. 2013.

[8] J. Wang, Q. Gao, Y. Yu, H. Wang, and M. Jin, "Toward robust indoor localization based on Bayesian filter using chirp-spread-spectrum ranging," IEEE Trans. Ind. Electron., vol. 3, no. 59, pp. 1622–1629, Mar. 2012.

[9] Crossbow Inc., T. Datasheet. [Online]. Available: http://www.xbow.com

[10] H. Ma, C. Zeng, and C. X. Ling, "A reliable people counting system via multiple cameras," *ACM Trans. Intell. Syst. Technol.*, vol. 3, no. 2, p. 31, Feb. 2012.

[11] P. Cheng, F. Zhang, J. Chen, Y. Sun, and X. Shen, "A distributed TDMA scheduling algorithm for target tracking in ultrasonic sensor networks," *IEEE Trans. Ind. Electron.*, vol. 60, no. 9, pp. 3836–3845, Sep. 2013.

[12] E. J. Candes and M. B. Wakin, "An introduction to compressive sampling," *IEEE Signal Process. Mag.*, vol. 25, no. 2, pp. 21–30, Mar. 2008.

[13] D. Needell and R. Vershynin, "Signal recovery from incomplete, inaccurate measurements via regularized orthogonal matching pursuit," *IEEE J. Sel. Topics Signal Process.*, vol. 4, no. 2, pp. 310–316, Apr. 2010.

[14] D. Polani, "Kullback–Leibler divergence," *Encyclopedia Syst. Biol.*, pp. 1087–1088, 2013.

[15] M. Gangeh *et al.*, "Categorizing extent of tumour cell death response to cancer therapy using quantitative ultrasound spectroscopy and maximum mean discrepancy," *IEEE Trans. Med. Imag.*, pp. 268–272, Jun. 2014.

[16] X. Zhu, J. Kandola, Z. Ghahramani, and J. D. Lafferty, "Nonparametric transforms of graph kernels for semi-supervised learning," in *Proc. Adv. Neural Inf. Process. Syst.*, 2004, pp. 1641–1648.

[17] M. S. Bazaraa, H. D. Sherali, and C. M. Shetty, *Nonlinear Programming: Theory and Algorithms*. New York, NY, USA: Wiley, 2013.

[18] A. F. Molisch, *Wireless Communications*, vol. 15. New York, NY, USA: Wiley, 2010.

[19] R. O. Duda, P. E. Hart, and D. G. Stork, *Pattern Classification*. New York, NY, USA: Wiley, 2012.

[20] M. Elad, *Sparse, Redundant Representations: From Theory to Applications in Signal, Image Processing*. New York, NY, USA: Springer-Verlag, 2010.

[21] B. Zhang *et al.*, "Sparse target counting, localization in sensor networks based on compressive sensing," in *Proc. 30th IEEE INFOCOM*, Shanghai, China, Apr. 2013, pp. 2255–2263.

[22] W. R. Heinzelman, A. Chandrakasan, and H. Balakrishnan, "Energy-efficient communication protocol for wireless microsensor networks," in *Proc. 33rd Annu. Hawaii Int. Conf. Syst. Sci.*, 2000, pp. 10–20.

[23] E. J. Candes, J. K. Romberg, and T. Tao, "Stable signal recovery from incomplete, inaccurate measurements," *Commun. Pure Appl. Math.*, vol. 59, no. 8, pp. 1207–1223, Aug. 2006.

[24] W. Xi, J. Z. Zhao, X. Y. Li *et al.*, "Electronic frog eye: Counting crowd using wifi," in *Proc. 33rd IEEE INFOCOM*, Toronto, ON, Canada, Apr. 2014, pp. 361–368.

Dingyi Fang received the Ph.D. degree in computer application technology from Northwestern Polytechnical University, Xi'an, China, in 2001.

He is currently a Professor with the School of Information Science and Technology, Northwest University, Xi'an. His current research interests include mobile computing and distributed computing systems, network and information security, and wireless sensor networks.

Chase Qishi Wu received the B.S. degree in remote sensing from Zhejiang University, Hangzhou, China, in 1995, the M.S. degree in geomatics from Purdue University, West Lafayette, IN, USA, in 2000, and the Ph.D. degree in computer science from Louisiana State University, Baton Rouge, LA, USA, in 2003.

He is currently with the School of Information Science and Technology, Northwest University, Xi'an, China. He is also currently an Associate Professor with the Department of Computer Science, The University of Memphis, Memphis, TN, USA. His research interests include big data, distributed computing, computer networks, sensor networks, scientific visualization, and cyber security.

Ju Wang received the B.S. degree in information engineering from Northwest University, Xi'an, China, in 2010, where he is currently working toward the Ph.D. degree in the School of Information Science and Technology.

His current research interests include localization, ubiquitous computation, signal processing, and routing design for wireless networks.

Zhe Yang received the B.S. degree in information engineering from Xi'an Jiaotong University, Xi'an, China, in 2005, and the Ph.D. degree in electrical and computer engineering from the University of Victoria, Victoria, BC, Canada, in 2013.

He is currently an Associate Professor with the School of Computer Science, Northwestern Polytechnical University, Xi'an. His current research interests include cross-layer design, scheduling and resources allocation for wireless networks, and synchronization.

Xiaojiang Chen (M'14) received the Ph.D. degree in computer software and theory from Northwest University, Xi'an, China, in 2010.

He is currently a Professor with the School of Information Science and Technology, Northwest University. His current research interests include localization and performance issues in wireless ad hoc, mesh, and sensor networks and named data networks.

Tianzhang Xing received the B.S. degree in information engineering from Xidian University of Electronic Science and Technology, Xi'an, China, in 2004. He is currently working toward the Ph.D. degree in the School of Information Science and Technology, Northwest University, Xi'an.

His current research interests include signal processing, localization, and Internet of things.